INORGANIC CHEMISTRY FRONTIERS

RESEARCH ARTICLE

Published on 03 September 2026
Licensed under CC-BY 4.0

Cite this: DOI: 10.1039/d6qi01256f

Super-flexible coordination: the metal matters

Cedric Uhlmann,[a] Steven Kebernik,[a] Luca Münzfeld,[a] Tim P. Seifert,[a] Ralf Köppe[a] and Peter W. Roesky[a,b]*

Herein, we report a unique tripodal system, a tin-chelated trisphosphine oxide scorpionate ligand that coordinates to hard metal atoms through the oxygen atoms and, upon full skeletal rearrangement, to soft metals through the phosphorus atoms. The reactions of the previously reported potassium salt [κ^3O-Sn(P(O)Ph$_2$)$_3$K] with rare-earth complexes based on the cyclooctatetraenediide ligand yielded the compounds [κ^3O-Sn(P(O)Ph$_2$)$_3$Ln^{III}(η^8-Cot)] (Ln = Y, Ce, Tb, Er; Cot = $C_8H_8^{2-}$) and [κ^3O-Sn(P(O)Ph$_2$)$_3$Ln^{III}(η^8-Cot^{TIPS})] (Ln = Y, Dy, Er; Cot^{TIPS} = 1,4-(iPr$_3$Si)$_2$C$_8$H$_6^{2-}$), in which the trivalent lanthanide ions are coordinated by the oxygen atoms, analogous to the potassium ions in the starting material. The reactions of the potassium salt and transition metal chlorides led to the isolation of the compounds [κ^3P-Sn(P(O)Ph$_2$)$_3$MCl] (M = Co, Fe). Interestingly, an *in situ* ligand rearrangement was observed for the transition metals, whereby the arrangement of the P(O)Ph$_2$ groups inverted. This results in a coordination of the oxygen atoms to the tin atom, while the phosphorus atoms bind to the d-metal ions. Quantum chemical calculations were performed to rationalize this observation.

Received 6th June 2026,
Accepted 10th August 2026

DOI: 10.1039/d6qi01256f

rsc.li/frontiers-inorganic

Introduction

Tripodal scorpionate ligands are widely used in various fields of catalysis, organometallic chemistry, and materials science due to their versatility.[2–4] These ligands are particularly advantageous in combination with transition metals, as they can effectively stabilize the complexes and facilitate the regulation of reactivity at the metal center.[2,5,6] In general, scorpionate ligands feature three identical or similar side groups into which various donor atoms such as sulfur (Fig. 1, **I**),[1] phosphorus (Fig. 1, **II**),[2,5] nitrogen (Fig. 1, **III**),[7] or oxygen (Fig. 1, **IV**)[8] are incorporated and which are linked by a central atom X (*e.g.* B, C, N, Si, P, Co)[1,2,5,7,8] acting as a bridgehead (Fig. 1). If the central atom also has donor properties, these ligands can exhibit not only tridentate but also tetradentate coordination (Scheme 1 and Fig. 1, **I**).[1] The best-known tripodal ligand is probably the tris(pyrazolyl)borate ligand (Fig. 1, **III**) established by Trofimenko, who also coined the term "scorpionate ligand".[7] This ligand is primarily used in the synthesis of transition metal complexes,[9] but also in lanthanide complexes.[10] Usually, scorpionate ligands are stable and do not show rearrangements. Only a few examples are known in which a skeletal rearrangement of one pyrazolyl group was seen. For example, coordination of two equivalents of [HB(3-isopropylpyrazol-1-yl)$_3$]$^-$ to Co^{2+} leads, due to a steric clash, to a setup in which one ring of each ligand, with the isopropyl group, is located at the 5-position.[11] A similar flip of one ring has been seen in other complexes,[12,13] while, to the best of our knowledge, a skeletal rearrangement of all three arms had not been reported.

The versatile coordination chemistry of phosphorus makes it an intriguing candidate for use as a donor site in tripodal ligands, resulting in advantageous properties. These include its high affinity towards transition metals, flexible coordination, and easy tunability in terms of its electronic and steric properties. In addition, phosphorus-containing ligands with

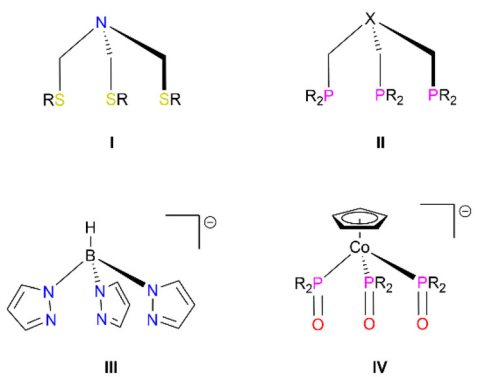

Fig. 1 Selected tripodal ligands: **I**, N(CH$_2$SR)$_3$ (R = Me, Et);[1] **II**, [X(LPR$_2$)$_3$] (X = B, BPh, CR, N, Si$^-$, P; L = CH$_2$, C$_2$H$_4$ C$_6$H$_4$; R = Me, iPr, Ph);[2,5] **III**, [HB(C$_3$N$_2$H$_3$)$_3$]$^-$;[7] and **IV**, [C$_5$H$_5$Co{P(O)R$_2$}$_3$]$^-$ (R = OMe).[8]

[a]*Institute of Inorganic Chemistry, Karlsruhe Institute of Technology, Engesserstr. 15, 76131 Karlsruhe, Germany. E-mail: roesky@kit.edu*
[b]*Institute of Nanotechnology, Karlsruhe Institute of Technology, Kaiserstr. 12, 76131 Karlsruhe, Germany*

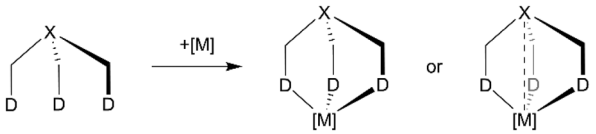

Scheme 1 Structural motifs of tridentate and quadridentate ligands coordinating to a metal atom (D = donor site; X = bridgehead of a tripodal ligand without (left) and with donor properties (right)).

multiple donor sites often exhibit chelating properties, which can increase the stability and reactivity of the resulting metal complexes.[2,5,6] A well-established example of this is the ligand $[C_5H_5Co\{P(O)(OMe)_2\}_3]^-$ (L^{Co}), (Fig. 1, **IV**), established by Kläui *et al.*,[8] which is widely used in both transition metal and lanthanide chemistry, *e.g.*, $[(L^{Co})_2M^{II}]$ (M = Co, Cu),[14] $[(L^{Co})Tc^{IV}Cl_3]$[15] and $[\{(L^{Co})_2Ln^{III}\}^+Cl^-]$ (Ln = Nd, Eu, Tb, Yb).[16]

Herein, we showcase the synthesis and characterization of rare-earth complexes (Ln^{III} = Y, Ce, Tb, Dy, Er) and transition metals (Co^{II}, Fe^{II}), which are coordinated by an anionic tripodal tin-chelated trisphosphine oxide scorpionate ligand $[Sn(P(O)Ph_2)_3]^-$.[17] We have previously reported on the synthesis of this ligand.[18] $[Sn(P(O)Ph_2)_3]^-$ coordinates to hard metal atoms through the oxygen atoms and, upon full skeletal rearrangement, to the softer transition metals through the phosphorus atoms.

Results and discussion

Rare-earth complexes[17]

Recently, we reported the coordination of the scorpionate ligand $\{Sn(P(O)Ph_2)_3\}^-$ to monoporphyrinate rare-earth complexes.[18] This resulted in a series of seven-coordinate complexes with the general formula $[(TPP)Ln(PPh_2O)_3Sn]$ (Ln = Y, La, Dy, Er, Ho, Yb; TPP = 5,10,15,20-tetraphenylporphyrinate). In this contribution, the porphyrinate ligand was formally replaced by cyclooctatetraenediide (Cot) to further investigate the fundamental coordination chemistry of this novel ligand with a coligand that provides a more open coordination environment with reduced steric constraints, thereby allowing for a more detailed understanding of the coordination preferences.

The Ln^{III}-Cot building blocks $[(\eta^8\text{-Cot})Ln^{III}I(thf)_2]$ (Ln = Y, Ce, Tb, Er; Cot = $C_8H_8^{2-}$) were synthesized according to the method established by Mashima *et al.*[19] Subsequent reactions of $[(\eta^8\text{-Cot})Ln^{III}I(thf)_2]$ with equimolar amounts of the potassium salt **1** gave rise to the heteroleptic compounds $[\kappa^3O\text{-}Sn(P(O)Ph_2)_3Ln^{III}(\eta^8\text{-Cot})]$ (**2-Ln**) (Scheme 2) in moderate crystalline yields of 25–35% as yellow and orange crystals.

Single crystals suitable for X-ray diffraction analysis of compounds **2-Ln** were obtained after extraction with hot THF and cooling of the saturated solution to room temperature. The isomorphous class of compounds crystallizes with one molecule of **2-Ln** and two molecules of THF in the asymmetric unit (Fig. 2). The central rare-earth ion is coordinated by an η^8-Cot and a $\kappa^3O\text{-}Sn(P(O)Ph_2)_3$ ligand. The P–O bond lengths range from 1.516(3) Å (**2-Tb**) to 1.5324(14) Å (**2-Y**) and are within the range of P–O double bonds.[20] The Ln–Ct_{Cot} distances range from 2.0130(3) Å (**2-Ce**) to 1.8277(3) Å (**2-Er**), corresponding to the decreasing ionic radii, and are comparable to the Ln–Ct_{Cot} distances of similar compounds.[21,22] Compared to the analogous TPP complexes, the **2-Ln** (Ln = Y, Er) complexes differ primarily in the Ct_{Cot}–Ln–Sn angles (**2-Y:** 172.453(10)°, **2-Er:** 172.22(1)°), which are both 4.45° smaller compared to the Ct_{N4}–Ln–Sn angles and therefore render these structures slightly more bent, which results from the lower steric hindrance of the Cot ligand. All other binding parameters are nearly identical. Conclusive NMR spectra could not be obtained due to the low solubility of compound class **2** in common organic solvents at ambient temperature.

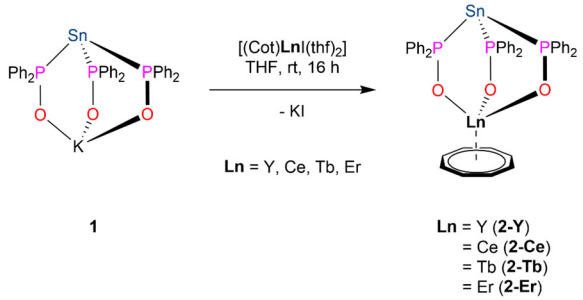

Scheme 2 Synthesis of the rare earth complexes $[\kappa^3O\text{-}Sn(P(O)Ph_2)_3Ln^{III}(\eta^8\text{-Cot})]$ **2-Ln** (Ln = Y, Ce, Tb, Er).

To facilitate NMR spectroscopic investigations and obtain higher yields of this novel class of compounds, we attempted to introduce a more sterically demanding co-ligand with better solubility in organic solvents. This was achieved by using $[(\eta^8\text{-}Cot^{TIPS})Ln^{III}(BH_4)(thf)]$ (Ln^{III} = Y, Dy, Er; Cot^{TIPS} = 1,4-$(iPr_3Si)_2C_8H_6^{2-}$)as the starting material.[22–25]

The synthesis followed the above-described procedure for the unsubstituted compounds **2-Ln**. Equimolar amounts of potassium salt **1** and the half-sandwich compound $[(\eta^8\text{-}Cot^{TIPS})Ln^{III}(BH_4)(thf)]$ were reacted in a salt-elimination reaction (Scheme 3). After subsequent extraction with toluene, the compounds $[\kappa^3O\text{-}Sn(P(O)Ph_2)_3Ln^{III}(\eta^8\text{-}Cot^{TIPS})]$ **3-Ln** (Ln = Y, Dy, Er) were obtained in crystalline yields ranging from 39% to 52%.

Single crystals suitable for X-ray diffraction analysis of compounds **3-Ln** were obtained by storing a saturated toluene solution at −30 °C. The isomorphous compound class **3-Ln** crystallizes with one formula unit in each asymmetric unit (Fig. 3). Similar to compounds **2-Ln**, the central rare-earth ion is coordinated by an $\eta^8\text{-}Cot^{TIPS}$ and a $\kappa^3O\text{-}Sn(P(O)Ph_2)_3$ ligand. In complexes **3-Ln**, an expansion of the Ct_{Cot}–Ln–Sn angle (avg. 175.1°) is observed compared to compounds **2-Ln** (avg. 171.7°), while the P–O and $Ct_{CotTIPS}$–Ln^{III} distances remain essentially unchanged.

The yttrium complex **3-Y** was used for NMR spectroscopic investigations due to its diamagnetic properties. In the ^1H NMR spectrum (Fig. S1), the signals of the phenyl groups were

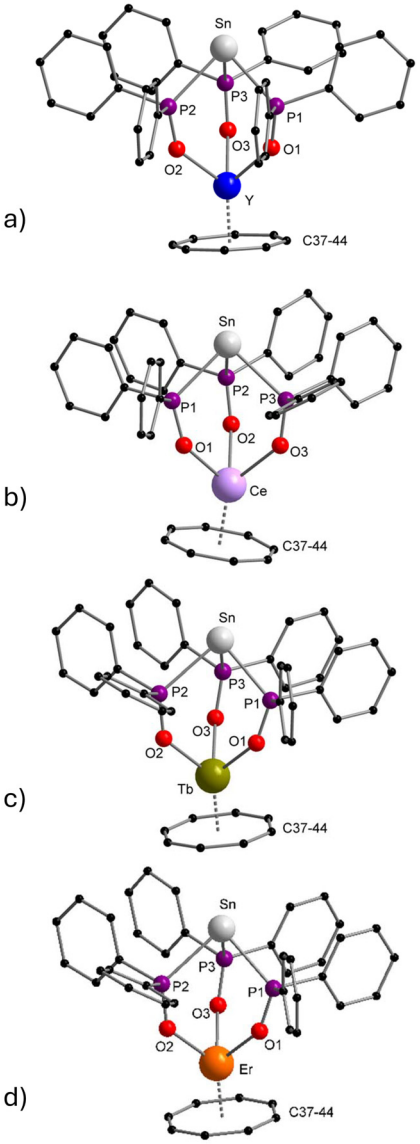

Fig. 2 Molecular structures of $[\kappa^3O\text{-Sn(P(O)Ph}_2)_3\text{Ln}^{III}(\eta^8\text{-Cot})]$ **2-Y** (a), **2-Ce** (b), **2-Tb** (c) and **2-Er** (d) in the solid state. Hydrogen atoms and non-coordinating THF molecules are omitted for clarity. Selected distances [Å] and angles [°]: **2-Y**: Sn–P1 2.6100(5), Sn–P2 2.6337(5), Sn–P3 2.6465(5), P1–O1 1.5295(15), P2–O2 1.5289(15), P3–O3 1.5324(14), Y–O1 2.2349(14), Y–O2 2.2433(15), Y–O3 2.2624(13), Y–Ct_{Cot} 1.8559(3), Sn–Y 4.5817(4); Sn–P1–O1 115.07(6), Sn–P2–O2 116.33(6), Sn–P3–O3 121.21(6), Ct_{Cot}–Y–O1 125.91(4), Ct_{Cot}–Y–O2 127.96(4), Ct_{Cot}–Y–O3 134.61(4). **2-Ce**: Sn–P1 2.6107(7), Sn–P2 2.6330(8), Sn–P3 2.6431(8), P1–O1 1.532(2), P2–O2 1.528(2), P3–O3 1.530(2), Ce–O1 2.362(2), Ce–O2 2.380(2), Ce–O3 2.392(2), Ce–Ct_{Cot} 2.0130(3), Sn–Ce 4.6789(4); Sn–P1–O1 115.80(8), Sn–P2–O2 117.29(8), Sn–P3–O3 121.45(7), Ct_{Cot}–Ce–O1 124.93(5), Ct_{Cot}–Ce–O2 129.11(5), Ct_{Cot}–Ce–O3 138.07(5). **2-Tb**: Sn–P1 2.5846(9), Sn–P2 2.6245(9), Sn–P3 2.6184(9), P1–O1 1.516(3), P2–O2 1.521(3), P3–O3 1.518(3), Tb–O1 2.248(2), Tb–O2 2.278(2), Tb–O3 2.259(2), Tb–Ct_{Cot} 1.8626(3), Sn–Tb 4.5627(4); Sn–P1–O1 115.36(10), Sn–P2–O2 121.24(10), Sn–P3–O3 116.76(10), Ct_{Cot}–Tb–O1 125.09(5), Ct_{Cot}–Tb–O2 135.50(6), Ct_{Cot}–Tb–O3 128.24(6). **2-Er**: Sn–P1 2.5996(6), Sn–P2 2.6381(6), Sn–P3 2.6280(6), P1–O1 1.524(2), P2–O2 1.530(2), P3–O3 1.525(2), Er–O1 2.219(2), Er–O2 2.247(2), Er–O3 2.231(2), Er–Ct_{Cot} 1.8277(3), Sn–Er 4.5608(3); Sn–P1–O1 115.24(7), Sn–P2–O2 121.14(7), Sn–P3–O3 116.65(7), Ct_{Cot}–Er–O1 125.30(4), Ct_{Cot}–Er–O2 134.57(5), Ct_{Cot}–Er–O3 127.99(4).

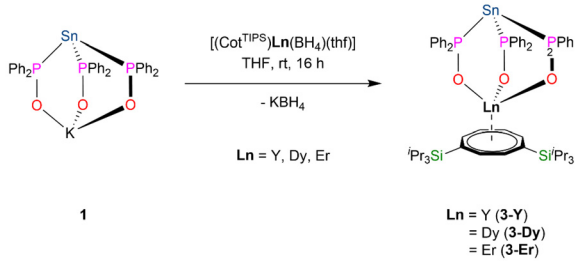

Scheme 3 Synthesis of the rare earth complexes $[\kappa^3O\text{-Sn(P(O)Ph}_2)_3\text{Ln}^{III}(\eta^8\text{-Cot}^{TIPS})]$ **3-Ln** (Ln = Y, Dy, Er) featuring a triisopropylsilyl-substituted Cot co-ligand.

observed at δ = 7.17 ppm and δ = 7.04 ppm. Compared to potassium salt **1**, these are shifted to lower resonance frequencies.[18] In the $^{31}P\{^1H\}$ NMR spectrum (Fig. S4), a doublet resonance at δ = 68.8 ppm was observed due to coupling of the phosphorus nuclei with the yttrium nucleus with a coupling constant of $^2J_{PY}$ = 6.7 Hz, as well as the corresponding satellites due to coupling with the two tin isotopes ^{117}Sn and ^{119}Sn. Compared to potassium salt **1** (δ = 54.7 ppm), the resonance is shifted to higher resonance frequencies.[18] The $^{119}Sn\{^1H\}$ NMR spectrum (Fig. S6) shows a quartet at a chemical shift of δ = −438.5 ppm with a coupling constant of $^1J_{PSn}$ = 1561 Hz, which is shifted by 228.9 ppm to lower resonance frequencies compared to potassium salt **1** (δ = −209.6 ppm).[18] The resonance of the ^{89}Y nucleus could only be detected using two-dimensional $^1H/^{89}Y$ HMBC experiments at a chemical shift of δ = −39.4 ppm (Fig. S5).

Transition metal complexes[17]

In order to extend the coordination chemistry of this scorpionate ligand to transition metals, $[\kappa^3O\text{-Sn(P(O)Ph}_2)_3K]$ (**1**) was treated with equimolar amounts of $M^{II}Cl_2$ (M = Co, Fe). This gave rise to the heteroleptic compounds $[\kappa^3P\text{-Sn(P(O)Ph}_2)_3M^{II}Cl]$ (M = Co (**4-Co**), Fe (**4-Fe**)) in yields of 66% and 71%, respectively (Scheme 4).

Single crystals suitable for X-ray diffraction analysis of compounds **4-M** were obtained by recrystallization from hot toluene (Fig. 4). The metal atom is coordinated in a slightly distorted tetrahedral arrangement by three phosphorus atoms and one chlorine atom. While M–O-coordination is evident from precursor **1** and in complexes **2-Ln** and **3-Ln**, M–P-coordination is observed in **4-M**. The ligand in **4-M** is therefore coordinated in a tridentate coordination mode to the cobalt or iron atom, whereby the arrangement of the $P(O)Ph_2$ units from $Sn\text{–}P(Ph_2)\text{–}O\text{–}K$ to $Sn\text{–}O\text{–}P(Ph_2)\text{–}M$ is inverted by an *in situ* ligand skeletal rearrangement during the reaction. Compared to compound **1**, the P–O bonds in compound class **4-M** are slightly longer, ranging between 1.550(7) Å and 1.569(3) Å.[18] The observed skeletal rearrangement of all arms with a tripodal scorpionate ligand is, to the best of our knowledge, unique.

NMR spectroscopic investigations were carried out for compound class **4-M**, but due to the paramagnetic behavior of **4-**

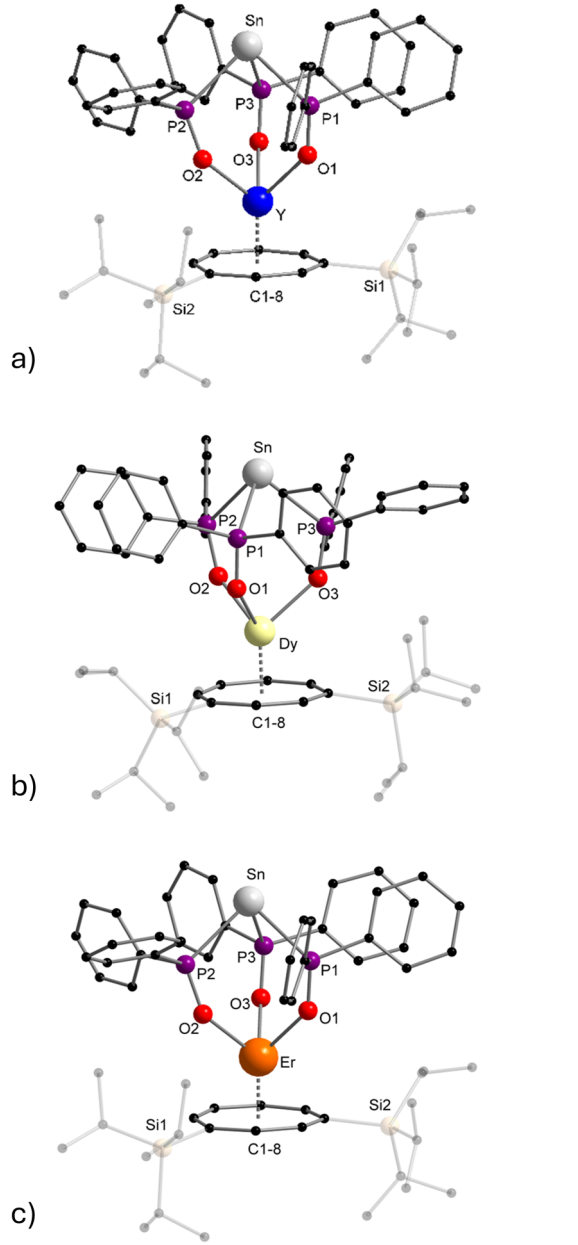

Fig. 3 Molecular structures of [κ^3*O*-Sn(P(O)Ph_2)$_3$$Ln^{III}$($\eta^8$-$Cot^{TIPS}$)] **3-Y** (a), **3-Dy** (b) and **3-Er** (c) in the solid state. Hydrogen atoms are omitted for clarity. Selected distances [Å] and angles [°]: **3-Y**: Sn–P1 2.6391(9), Sn–P2 2.6070(10), Sn–P3 2.6134(10), P1–O1 1.526(2), P2–O2 1.532(2), P3–O3 1.525(2), Y–O1 2.265(2), Y–O2 2.251(2), Y–O3 2.262(2), Y–$Ct_{CotTIPS}$ 1.8365(3), Sn–Y 4.5913(5); Sn–P1–O1 118.23(10), Sn–P2–O2 115.04(10), Sn–P3–O3 116.13(10), $Ct_{CotTIPS}$–Y–O1 133.93(6), $Ct_{CotTIPS}$–Y–O2 128.98(6), $Ct_{CotTIPS}$–Y–O3 127.96(6). **3-Dy**: Sn–P1 2.6438(9), Sn–P2 2.6161(8), Sn–P3 2.6113(10), P1–O1 1.528(3), P2–O2 1.533(3), P3–O3 1.530(3), Dy–O1 2.285(2), Dy–O2 2.282(2), Dy–O3 2.275(2), Dy–$Ct_{CotTIPS}$ 1.8464(3), Sn–Dy 4.6154(5); Sn–P1–O1 118.48(9), Sn–P2–O2 116.68(9), Sn–P3–O3 115.41(10), $Ct_{CotTIPS}$–Dy–O1 134.22(6), $Ct_{CotTIPS}$–Dy–O2 127.74(6), $Ct_{CotTIPS}$–Dy–O3 129.23(6). **3-Er**: Sn–P1 2.6457(8), Sn–P2 2.6118(9), Sn–P3 2.6157(8), P1–O1 1.527(2), P2–O2 1.530(2), P3–O3 1.528(2), Er–O1 2.260(2), Er–O2 2.251(2), Er–O3 2.258(2), Er–$Ct_{CotTIPS}$ 1.8188(3), Sn–Er 4.5933(5); Sn–P1–O1 118.33(9), Sn–P2–O2 115.37(9), Sn–P3–O3 116.22(8), $Ct_{CotTIPS}$–Er–O1 133.60(6), $Ct_{CotTIPS}$–Er–O2 128.93(6), $Ct_{CotTIPS}$–Er–O3 127.91(6).

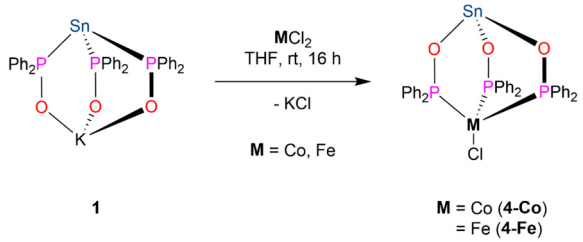

Scheme 4 Synthesis of transition metal complexes [κ^3*P*-Sn(P(O)Ph_2)$_3$$M^{II}$Cl] **4-Co** and **4-Fe** by an *in situ* ligand rearrangement.

Co, no meaningful NMR spectra could be obtained except for the $^{31}P\{^1H\}$ spectrum. In the ^1H NMR spectrum of the diamagnetic compound **4-Fe** (Fig. S8), the signals of the phenyl groups were observed at δ = 7.42 ppm and δ = 6.93–6.83 ppm. Compared to potassium salt **1**, these are shifted to lower resonance frequencies.[18] In the $^{31}P\{^1H\}$ NMR spectrum of **4-Fe** (Fig. S10), a signal at δ = 144.9 ppm with corresponding satellites was observed due to coupling with the two tin isotopes ^{117}Sn and ^{119}Sn,[26] while in the $^{31}P\{^1H\}$ NMR spectrum of **4-Co**

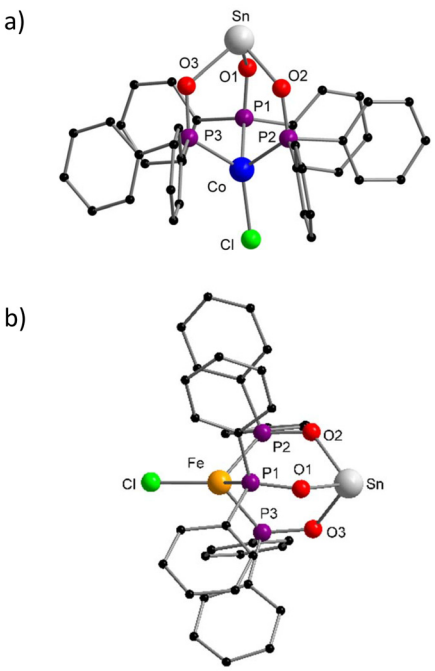

Fig. 4 Molecular structures of [κ^3*P*-Sn(P(O)Ph_2)$_3$$M^{II}$Cl] **4-Co** (a) and **4-Fe** (b) in the solid state from different angles. Hydrogen atoms are omitted for clarity. Selected distances [Å] and angles [°]: **4-Co**: Sn–O1 2.130(3), Sn1–O2 2.115(4), Sn1–O3 2.089(3), P1–O1 1.556(4), P2–O2 1.553(4), P3–O3 1.569(3), Co1–P1 2.1372(14), Co–P2 2.1242(14), Co–P3 2.218(2), Co–Cl 2.1595(14), Sn–Co 3.9426(5); Sn–O1–P1 129.58(14), Sn–O2–P2 128.22(14), Sn–O3–P3 126.76(15), P1–Co–Cl 119.06(4), P2–Co–Cl 119.45(4), P3–Co–Cl 130.29(4). **4-Fe**: Sn1–O1 2.087(6), Sn1–O2 2.099(6), Sn1–O3 2.075(6), P1–O1 1.554(7), P2–O2 1.550(7), P3–O3 1.554(7), Fe1–P1 2.115(3), Fe1–P2 2.110(3), Fe1–P3 2.110(3), Fe1–Cl1 2.127(3), Sn1–Fe1 3.9588(14); Sn1–O1–P1 126.4(4), Sn1–O2–P2 127.7(4), Sn1–O3–P3 127.5(4), P1–Fe1–Cl1 128.44(11), P2–Fe1–Cl1 122.17(11), P3–Fe1–Cl1 122.50(11).

(Fig. S7), a signal without satellites was observed at δ = −14.9 ppm. Compared to potassium salt **1** (δ = 54.7 ppm), the resonances are shifted to both significantly higher (**4-Fe**) and significantly lower (**4-Co**) resonance frequencies.[18] The ^{119}Sn {^{1}H} NMR spectrum of **4-Fe** shows a singlet at a chemical shift of δ = −466.6 ppm (Fig. S11), unlike the quartet signal of potassium salt **1** (δ = −209.6 ppm), which was shifted to lower resonance frequencies, with a coupling constant of $^1J_{PSn}$ = 1621 Hz.[18] These results clearly show that compounds **4-M** with the rearranged ligand are stable in solution.

The subsequent reaction of half a stoichiometric equivalent of $M^{II}Cl_2$ (M = Co, Fe) with compound **1** did not result in the homoleptic compounds [(κ^3*P*-Sn(P(O)Ph$_2$)$_3$)$_2$M] as expected but only led to the isolation of compounds **4-Co** and **4-Fe**. The steric repulsion of the phenyl rings extending beyond the metal atom is assumed to prevent the reaction of compound **4-M** with another equivalent of compound **1**.

Finally, we compared the IR spectra of all the compounds. By investigating the eigenvectors obtained from the theoretical frequency analyses (*v. i.*), we were able to identify the theoretical P–O stretching vibrations in the IR spectra of **1**, **2-Y**, **4-Fe**, and **4-Co** and assign them to the corresponding signals in the experimental spectra (Table S17 and Fig. S36). Indeed, a distinct red shift of about 130 cm^{-1} in the P–O stretching vibrations was observed when moving from the coordination mode found in **1** or **2-Y** to that found in **4-Fe** or **4-Co**.

Quantum chemical calculations

Theoretical calculations were carried out using the program package TURBOMOLE[27] (functional RI-BP 86,[28–30] basis sets def2-TZVP,[31] dispersion correction D3[32]) to investigate the bonding situation in the yttrium complex **2-Y** and in the iron compound **4-Fe**. The results were compared with those of the potassium salt **1**. The theoretical structures of all investigated molecules and multiplicities were determined by geometry optimizations without symmetry constraints (C_1). Frequency calculations performed using the AOFORCE[33] routine confirmed all of these geometries as true minima. The energy situation is determined by differences in the total energy values in every case.

First, both possible structural isomers of the existing yttrium complex, **2-Y** (Y–O coordination) and the hypothetical yttrium complex **2-Y′** (Y–P coordination), were theoretically investigated. Complex **2-Y**, featuring the same M–O-coordination as the ligand seen in the potassium salt **1**, is 106.5 kJ mol^{-1} (see Table S13) more stable than the other structural isomers containing metal–phosphorus bonds, as found in the iron and cobalt complexes (**4-Fe** and **4-Co**). The bonding characteristics of **2-Y** and **2-Y′** were compared using an Ahlrichs–Heinzmann population analysis, with shared electron numbers (SENs) serving as a measure of covalent bond strength and Q as atomic partial charge.[34,35] Furthermore, the local force constants F_l[36] were calculated using the lmodea-nano plugin of the visualization program PyMOL.[37] These force constants are a sensitive measure of covalent bond strength.[38] The partial atomic charges that form the ligand backbone (Sn, O, and P) are in good agreement with those of potassium salt **1** (see Tables S14 and S16; **2-Y**: Q(Y) + 1.72, Q(Sn) − 0.24, Q(O) − 0.81 to −0.61, Q(P) + 0.80; **1**: Q(Sn) − 0.31, Q(O) − 0.75 to −0.61, Q(P) + 0.90). Accordingly, a localization of the molecular orbitals (MOs) using the Pipek–Mezey method[39] reveals no localized molecular orbital (LMO) that can be assigned to a Y–O bond with even a small covalent component. Therefore, we are confident that this bond is nearly entirely ionic. The stabilization of over 100 kJ mol^{-1} compared to the isomer with Y–P coordination **2-Y′** becomes clear when the respective P–O bonds are compared: in **2-Y**, this bond is significantly shorter than in the other structural isomer **2-Y′** (**2-Y**: d(P–O): 1.540 Å; **2-Y′**: d(P–O): 1.592–1.603 Å; see Table S16). This can be explained by increased π-bonding: the increased covalent bond strength is reflected in the increased SEN (P–O) as well as in the local force constant F_l(P–O) (**2-Y**: SEN 1.21, F_l 6.48 mdyn Å^{-1}; **2-Y′**: SEN 1.10 to 1.15, F_l 4.61–4.92 mdyn Å^{-1}).

According to the HSAB (hard and soft acids and bases) principle, the hard metal–hard O-donor coordination situation in **2-Y** is in good agreement with that of the potassium salt **1**.

Experimental investigations revealed a change in coordination in the iron compound **4-Fe** compared to the lanthanide compounds. For the corresponding theoretical investigations, the two conceivable structural isomers, **4-Fe** (Fe–P coordination) and the hypothetical **4-Fe′** (Fe–O coordination), were calculated, along with their different multiplicities of the associated low- and high-spin complexes, as well as the spin-crossover multiplicity of a distorted tetrahedral Fe^{2+} complex **4-Fe**. The Fe complex in the singlet state was found to represent the ground state (energy differences from the triplet state of 91.6 and the quintet state of +126.4 kJ mol^{-1}). The calculated structural data of the singlet ground state are in very good agreement with the experimental data.

On the other hand, the ground state of the hypothetical iron complex **4-Fe′**, coordinated analogously to potassium salt **1**, is formed as a high-spin complex *via* the quintet state. As expected, its energy is +198.5 kJ mol^{-1} higher than that of the actually formed compound **4-Fe**. The structural data of the ligand anion in this hypothetical compound align well with those of potassium salt **1**, suggesting a more ionic bonding situation between the metal cation and the ligand. Furthermore, by comparing the results of the Ahlrichs–Heinzmann population analyses of both possible isomers, the reason for the significantly greater stability of **4-Fe** compared to **4-Fe′** can be determined: while an Fe–P bond with a rather high SEN (0.84) is found in **4-Fe** (Fig. 5), the corresponding Fe–O bond in **4-Fe′** (SEN 0.27) is merely electrostatic in nature. However, the strengths of the covalent P–O bonds in both isomers are not as different as they are in the Y compounds (Fig. 5). This is particularly evident when comparing the local force constants (**4-Fe**: SEN(P–O): 1.03, F_l(P–O): 4.89; **4-Fe′**: SEN (P–O): 1.17, F_l(P–O): 5.36–5.69 mdyn Å^{-1}). The results for the two possible cobalt complexes, **4-Co** and **4-Co′**, are in very good agreement with those of the iron compound. Here, the cobalt complex (doublet ground state) is calculated to be

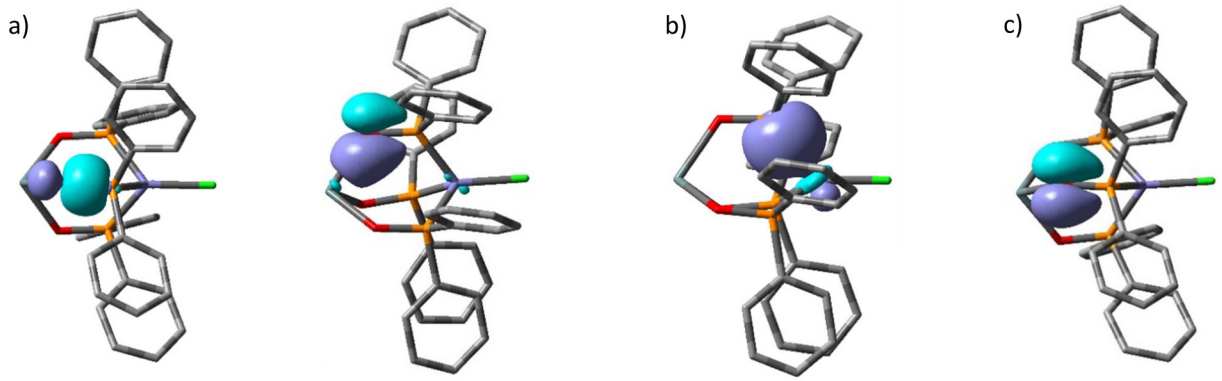

Fig. 5 Isosurface plots (values ± 0.06*e*) of the localized MOs of **4-Fe** showing (a) P–O (σ and π2), (b) Fe–P-, and (c) Sn–O-bonding (LMOs 83, 162, 128, 162).

−218.3 kJ mol^{-1} more stable than the ground state (quartet) of the other structural isomer (see the SI).

Compared to **4-Fe** and **4-Co**, the molecules **2-Y** and **1** possess significantly increased (theoretically determined) local force constants for the P–O bonds (see Tables S14–S16); consequently, this difference should be reflected in the IR spectra. Therefore, we investigated the eigenvectors obtained from the frequency analyses to identify the theoretical P–O stretching vibrations in the IR spectra of **1**, **2-Y**, **4-Fe**, and **4-Co** and to assign them to the corresponding signals in the experimental spectra. Indeed, the aforementioned distinct red shift of about 130 cm^{-1} in the P–O stretching vibrations is observed when moving from the coordination mode found in **1** or **2-Y** to that in **4-Fe** or **4-Co** (the data are given in Table S17). However, an analysis of the Sn–O stretching vibrations is not possible, as these are partly coupled with the transition metal–phosphorus motion, particularly in the cases of **4-Fe** and **4-Co**.

The bonding situation can therefore be summarized as follows: in **4-Fe**, the ligand generates a very strong ligand field upon metal–P coordination, resulting in a low-spin complex. In the hypothetical complex **4-Fe′** however, only a weak ligand field is generated. These findings align with the expected high stability of this soft metal–soft P coordination according to the HSAB principle.

Conclusions

In summary, we report on the unusual dynamic tripodal, tin-chelated trisphosphine oxide scorpionate ligand through the synthesis of a series of rare-earth and transition metal complexes. For the transition metal complexes [κ^3*P*-Sn(P(O)Ph$_2$)$_3$M^{II}Cl] **4-M** (M = Co, Fe), an unprecedented *in situ* ligand rearrangement was observed with the inversion of the P(O)Ph$_2$ arrangement, so that the coordination of the transition metals Co^{II} and Fe^{II} *via* the phosphorus atoms was seen. For the rare-earth complexes [κ^3*O*-Sn(P(O)Ph$_2$)$_3$Ln^{III}(η^8-Cot)] (**2-Ln**) (Ln = Y, Ce, Tb, Er) and [κ^3*O*-Sn(P(O)Ph$_2$)$_3$Ln(η^8-Cot^{TIPS})] **3-Ln** (Ln = Y, Dy, Er), no ligand rearrangement was observed. In this instance, coordination of the Ln^{III} ions occurred through the oxygen atoms, consistent with the observed behavior for the potassium salt. Investigations using quantum chemical calculations confirm the experimental findings.

Conflicts of interest

There are no conflicts to declare.

Data availability

Data for this paper (synthesis and characterization, NMR, Raman, and IR spectra, X-ray crystallography, and quantum chemical calculations) are available at radar4chem [**https://radar.products.fiz-karlsruhe.de/**; **https://doi.org/10.22000/n432431gy9nf2v13**].

Supplementary information (SI) is available. See DOI: **https://doi.org/10.1039/d6qi01256f**.

CCDC 2559271–2559279 contain the supplementary crystallographic data for this paper.[40a–i]

Acknowledgements

The authors gratefully acknowledge support from the Deutsche Forschungsgemeinschaft (DFG, German Research Foundation) through the Collaborative Research Centre “4f for Future” (CRC 1573 project number 471424360, project C1). The authors acknowledge support from the state of Baden-Württemberg through bwHPC and the German Research Foundation (DFG) through grant no. INST 40/575-1 FUGG (JUSTUS 2 cluster).

References

1 E. A. Ambundo, M.-V. Deydier, A. J. Grall, N. Aguera-Vega, L. T. Dressel, T. H. Cooper, M. J. Heeg, L. A. Ochrymowycz

and D. B. Rorabacher, Influence of coordination geometry upon copper(II/I) redox potentials. physical parameters for twelve copper tripodal ligand complexes, *Inorg. Chem.*, 1999, **38**, 4233–4242.
2 C. Bianchini, A. Meli, M. Peruzzini, F. Vizza and F. Zanobini, Tripodal polyphosphine ligands control selectivity of organometallic reactions, *Coord. Chem. Rev.*, 1992, **120**, 193–208.
3 X. Hu and K. Meyer, New tripodal N-heterocyclic carbene chelators for small molecule activation, *J. Organomet. Chem.*, 2005, **690**, 5474–5484.
4 L. F. Sánchez-Barba, A. Garcés, A. Lara-Sánchez, M. Navarro and D. González-Lizana, Main advances in the application of scorpionate-based catalytic systems for the preparation of sustainable polymers, *Chem. Commun.*, 2025, **61**, 1087–1103.
5 C. T. Saouma and J. C. Peters, M≡E and M=E complexes of iron and cobalt that emphasize three-fold symmetry (E = O, N, NR), *Coord. Chem. Rev.*, 2011, **255**, 920–937.
6 A. Aloisi, J.-C. Berthet, C. Genre, P. Thuéry and T. Cantat, Complexes of the tripodal phosphine ligands $PhSi(XPPh_2)_3$ (X = CH_2, O): Synthesis, structure and catalytic activity in the hydroboration of CO_2, *Dalton Trans.*, 2016, **45**, 14774–14788.
7 S. Trofimenko, Recent advances in poly (pyrazolyl) borate (scorpionate) chemistry, *Chem. Rev.*, 1993, **93**, 943–980.
8 W. Kläui, H. Otto, W. Eberspach and E. Buchholz, Die Michaelis-Arbusov-Reaktion als Zugang zu neuen Sauerstoff-Tripodliganden des Typs $[C_5R_5M\{P(O)(OCH_3)_2\}_3]^-$. Ligandfeldspektroskopische und koordinationschemische Charakterisierung der Liganden, *Chem. Ber.*, 1982, **115**, 1922–1933.
9 S. Liang, H. Wang, T. Deb, J. L. Petersen, G. T. Yee and M. P. Jensen, Structural and spectroscopic trends in a series of half-sandwich scorpionate complexes, *Inorg. Chem.*, 2012, **51**, 12707–12719.
10 T. Chowdhury, S. J. Horsewill, C. Wilson and J. H. Farnaby, Heteroleptic lanthanide(III) complexes: Synthetic utility and versatility of the unsubstituted bis-scorpionate ligand framework, *Aust. J. Chem.*, 2022, **75**, 660–675.
11 S. Trofimenko, J. C. Calabrese, P. J. Domaille and J. S. Thompson, Steric effects in polypyrazolylborate ligands. Poly (3-isopropylpyrazolyl) borates: Ligands of intermediate steric requirements, *Inorg. Chem.*, 1989, **28**, 1091–1101.
12 A. Looney and G. Parkin, Poly(pyrazolyl)hydroborato and poly(pyrazolyl)methane aluminium alkyl derivatives, *Polyhedron*, 1990, **9**, 265–276.
13 J. Calabrese and S. Trofimenko, Hydrotris (3-neopentylpyrazol-1-yl) borates: a new type of sterically hindered poly (pyrazolyl) borates, *Inorg. Chem.*, 1992, **31**, 4810–4814.
14 E. Dubler, L. Linowsky and W. Kläui, Molecular structures and solid-solid phase transitions of trinuclear $CpCo[P(O)(OR)_2]_3$ 2M complexes, *Transition Met. Chem.*, 1979, **4**, 191–198.
15 A. C. Grunwald, C. Scholtysik, A. Hagenbach and U. Abram, One ligand, one metal, seven oxidation states: Stable technetium complexes with the "Kläui ligand", *Inorg. Chem.*, 2020, **59**, 9396–9405.
16 K. J. H. Allen, E. C. Nicholls-Allison, K. R. D. Johnson, R. S. Nirwan, D. J. Berg, D. Wester and B. Twamley, Lanthanide complexes of the Kläui metalloligand, $CpCo(P{=}O(OR)_2)_3$. An examination of ligand exchange kinetics between isotopomers by electrospray mass spectrometry, *Inorg. Chem.*, 2012, **51**, 12436–12443.
17 C. Uhlmann, Ph.D. thesis, Karlsruher Institut für Technologie (KIT), 2024.
18 D. Jin, C. Uhlmann, E. K. Schneider, T. Seifert, D. Graf, S. Lebedkin, P. Weis, M. M. Kappes and P. W. Roesky, Tin-chelated trisphosphineoxide scorpionate rare-earth porphyrinate complexes: Synthesis and photophysical properties, *Inorg. Chem.*, 2024, **63**, 24762–24770.
19 K. Mashima, Y. Nakayama, A. Nakamura, N. Kanehisa, Y. Kai and H. Takaya, A new convenient preparation of monocyclooctatetraenyl-lanthanide complexes from metallic lanthanides and oxidants, *J. Organomet. Chem.*, 1994, **473**, 85–91.
20 F. H. Allen, O. Kennard, D. G. Watson, L. Brammer, A. G. Orpen and R. Taylor, Tables of bond lengths determined by X-ray and neutron diffraction. Part 1. Bond lengths in organic compounds, *J. Chem. Soc., Perkin Trans. 2*, 1987, S1–S19.
21 K. R. Meihaus and J. R. Long, Magnetic blocking at 10 K and a dipolar-mediated avalanche in salts of the bis(η_8-cyclooctatetraenide) complex $[Er(COT)_2]^-$, *J. Am. Chem. Soc.*, 2013, **135**, 17952–17957.
22 L. Münzfeld, X. Sun, S. Schlittenhardt, C. Schoo, A. Hauser, S. Gillhuber, F. Weigend, M. Ruben and P. W. Roesky, Introduction of plumbole to f-element chemistry, *Chem. Sci.*, 2022, **13**, 945–954.
23 L. Münzfeld, S. Gillhuber, A. Hauser, S. Lebedkin, P. Hädinger, N. D. Knöfel, C. Zovko, M. T. Gamer, F. Weigend and M. M. Kappes, Synthesis and properties of cyclic sandwich compounds, *Nature*, 2023, **620**, 92–96.
24 L. Münzfeld, A. Hauser, P. Hädinger, F. Weigend and P. W. Roesky, The archetypal homoleptic lanthanide quadruple-Decker—Synthesis, mechanistic studies, and quantum chemical investigations, *Angew. Chem., Int. Ed.*, 2021, **60**, 24493–24499.
25 A. Hauser, L. Münzfeld, C. Uhlmann, S. Lebedkin, S. Schlittenhardt, T.-T. Ruan, M. M. Kappes, M. Ruben and P. W. Roesky, It's not just the size that matters: Crystal engineering of lanthanide-based coordination polymers, *Chem. Sci.*, 2024, **15**, 1338–1347.
26 K. H. A. O. Starzewski, P. S. Pregosin and H. Rüegger, ^{31}P-, ^{119}Sn- and ^{195}Pt-NMR. Studies of trichlorostannate complexes of Pt(II) and Pd(II). $^2J(^{119}Sn, ^{117}Sn)$-values, *Helv. Chim. Acta*, 1982, **65**, 785–797.
27 TURBOMOLE V7.6 2021, a development of University of Karlsruhe and Forschungszentrum Karlsruhe GmbH, 1989-2007, TURBOMOLE GmbH, since 2007; available from **https://www.turbomole.org**.
28 J. P. Perdew, Density-functional approximation for the correlation energy of the inhomogeneous electron gas,

Phys. Rev. B: Condens. Matter Mater. Phys., 1986, **33**, 8822–8824.
29 J. P. Perdew, Erratum: Density-functional approximation for the correlation energy of the inhomogeneous electron gas, *Phys. Rev. B: Condens. Matter Mater. Phys.*, 1986, **34**, 7406.
30 A. D. Becke, Density-functional exchange-energy approximation with correct asymptotic behavior, *Phys. Rev. A*, 1988, **38**, 3098–3100.
31 F. Weigend and R. Ahlrichs, Balanced basis sets of split valence, triple zeta valence and quadruple zeta valence quality for H to Rn: Design and assessment of accuracy, *Phys. Chem. Chem. Phys.*, 2005, **7**, 3297.
32 S. Grimme, J. Antony, S. Ehrlich and H. Krieg, A consistent and accurate *ab initio*, parametrization of density functional dispersion correction (DFT-D) for the 94 elements H-Pu, *J. Chem. Phys.*, 2010, **132**, 154104.
33 P. Deglmann, F. Furche and R. Ahlrichs, An efficient implementation of second analytical derivatives for density functional methods, *Chem. Phys. Lett.*, 2002, **362**, 511–518.
34 R. Heinzmann and R. Ahlrichs, Population analysis based on occupation numbers of modified atomic orbitals (MAOs), *Theor. Chem. Acc.*, 1976, **42**, 33–45.
35 R. Ahlrichs and C. Ehrhardt, Chemische Bindung anschaulich: Populationsanalysen, *Chem. Unserer Zeit*, 1985, **19**, 120–124.
36 W. Zou, Y. Tao, M. Freindorf, D. Cremer and E. Kraka, Local vibrational force constants – From the assessment of empirical force constants to the description of bonding in large systems, *Chem. Phys. Lett.*, 2020, **748**, 137337.
37 Y. Tao, W. Zou, S. Nanayakkara and E. Kraka, LModeA-nano: A PyMOL plugin for calculating bond strength in solids, surfaces, and molecules via local vibrational mode analysis, *J. Chem. Theory Comput.*, 2022, **18**, 1821–1837.
38 R. Köppe and H. Schnöckel, GaGa- und AlFe-Mehrfachbindungen? Ein Interpretationsversuch auf der Grundlage von Kraftkonstanten, *Z. Anorg. Allg. Chem.*, 2000, **626**, 1095–1099.
39 J. Pipek and P. G. Mezey, A fast intrinsic localization procedure applicable for *ab initio* and semiempirical linear combination of atomic orbital wave functions, *J. Chem. Phys.*, 1989, **90**, 4916–4926.
40 (*a*) CCDC 2559271: Experimental Crystal Structure Determination, 2026, DOI: **10.5517/ccdc.csd.cc2rx44z**; (*b*) CCDC 2559272: Experimental Crystal Structure Determination, 2026, DOI: **10.5517/ccdc.csd.cc2rx450**; (*c*) CCDC 2559273: Experimental Crystal Structure Determination, 2026, DOI: **10.5517/ccdc.csd.cc2rx461**; (*d*) CCDC 2559274: Experimental Crystal Structure Determination, 2026, DOI: **10.5517/ccdc.csd.cc2rx472**; (*e*) CCDC 2559275: Experimental Crystal Structure Determination, 2026, DOI: **10.5517/ccdc.csd.cc2rx483**; (*f*) CCDC 2559276: Experimental Crystal Structure Determination, 2026, DOI: **10.5517/ccdc.csd.cc2rx494**; (*g*) CCDC 2559277: Experimental Crystal Structure Determination, 2026, DOI: **10.5517/ccdc.csd.cc2rx4b5**; (*h*) CCDC 2559278: Experimental Crystal Structure Determination, 2026, DOI: **10.5517/ccdc.csd.cc2rx4c6**; (*i*) CCDC 2559279: Experimental Crystal Structure Determination, 2026, DOI: **10.5517/ccdc.csd.cc2rx4d7**.

